

A Centroid Loss for Weakly Supervised Semantic Segmentation in Quality Control and Inspection Application

Kai Yao · Alberto Ortiz · Francisco Bonnin-Pascual

Received: date / Accepted: date

Abstract Process automation has enabled a level of accuracy and productivity that goes beyond human ability, and one critical area where automation is making a huge difference is the machine vision system. In this paper, a semantic segmentation solution is proposed for two scenes. One is the inspection intended for vessel corrosion detection, and the other is a detection system used to assist quality control on the surgery toolboxes prepared by the sterilization unit of a hospital. In order to reduce the time required to prepare pixel-level ground truth, this work focuses on the use of weakly supervised annotations (scribbles). Moreover, our solution integrates a clustering approach into a semantic segmentation network, thus reducing the negative effects caused by weakly supervised annotations. To evaluate the performance of our approach, two datasets are collected from the real world (vessels' structure and hospital surgery toolboxes) for both training and validation. According to the result of analysis, the approach proposed in this paper produce a satisfactory performance on two datasets through the use of weak annotations.

Keywords Quality Control · Inspection · Object Recognition · Weakly Supervised Semantic Segmentation

1 Introduction

Playing a crucial role in industrial production, quality control endows manufacturing companies with eco-

nomical advantages while contributing to their competitiveness. Nowadays, machine vision systems have emerged as a superior alternative to human labor in the field of quality control and are still developing on the course for lean and flexible industrial systems. With its capability to achieve high accuracy while ensuring throughput on the production line, the vision system has also helped to ensure efficient inspection and quality control.

The machine vision system, which is combined with Deep Learning technique, can produce consistent and accurate detection results. Deep Convolution Neural Networks (DCNN) have achieved an excellent performance in a variety of different computer vision tasks. Especially for the semantic segmentation of images, the DCNN-based approaches [5, 21] are more effective in improving the detection performance significantly than previously-proposed methods. Inspired by these approaches, this paper focuses on applying the DCNN-based semantic segmentation technology in two different tasks. One is an inspection system intended for vessel corrosion detection, and the other relates to a quality control task that is to detect several control items, which are the sterilization unit of a hospital places in boxes and bags containing surgery tools.

Taking into account the cost of shipbuilding and the performance of the ship, most vessels rely on high-strength steel materials for the design of its overall structure. In the marine environment, steel material is prone to severe corrosion, and the damage caused by corrosion may lead to substantial losses and even put the safety of crew members at risk in some cases. Therefore, it is essential to carry out corrosion detection to prevent the occurrence of engineering disaster. In the first row of Fig. 1, it shows three patterns of corroded as recorded in the inspection dataset. The quality control task is proposed to provide the evidence suggesting that the tools have undergone the required cleaning processes before surgery. The second and third row in Fig. 1,

This work is partially supported by projects ROBINS (EU-H2020, GA 779776), PGC2018-095709-B-C21 (MCIU/AEI/FEDER, UE), and PROCOE/4/2017 (Govern Balear, 50% P.O. FEDER 2014-2020 Illes Balears)

Kai Yao, Alberto Ortiz, Bonnin-Pascual
Department of Mathematics and Computer Science,
University of the Balearic Islands, Spain
Tel.: +34-971-17-3104
E-mail: {k.yao, alberto.ortiz, xisco.bonnin}@uib.es



Fig. 1 Objects to be detected. Three corrosion examples are shown in the first row. The tracked label, seal, three kinds of paper tape (black-, blue-, and pink-striped) and the internal filter are displayed from left to right, from the middle row to the bottom row.

from left to right and from top to bottom, the six kinds of items need to be detected in this system: the label/bar code used to track a box/bag of tools, the yellowish seal, the three kinds of paper tape which change to the black-, blue- and pink-striped appearance when the box/bag has been sterilized, and an internal filter which is placed inside some boxes and creates the white-dotted texture that can be observed (instead of black-dotted when the filter is not inside).

For most of DCNN-based semantic segmentation approaches, there are a large number of pixel-level annotations required to train the neural network, which is not only time-consuming but also demanding a lot of physical work of human. Although a powerful interactive tool [3] has been developed for annotating targets at the pixel level, which makes it sufficient for the user to draw a minimal polygon surrounding the target, it still takes a few minutes on average to mark the target area for one picture in the Quality Control dataset. Meanwhile, it is difficult for inexperienced staff to ensure accuracy in marking corrosion at the pixel level in the Inspection dataset. Thus, the development of an image segmentation application for our two tasks is considered through weak annotations.

Up to now, the Weakly Supervised Semantic Segmentation (WSSS) has been widely discussed. There are various forms of user interaction suitable for segmentation annotations, such image tags, scribbles, and bounding boxes. For the convenience of using scribbles, the need for accurate annotations is removed for users. Instead, they are required only to drag the cursor in the area of targets for drawing scribbles. In addition, it is easy to distinguish between categories of scribbles using different color. Although scribble annotations can provide accurate annotations for a

few pixels, it is too ambiguous to recognize the whole object. Therefore, the WSSS using scribble annotations differs from the other two types of weak annotations, and it shows a medium level of difficulty. In our case, the scribble annotations are easy to implement and have been identified as a user-friendly means of annotations.

Inspired by the ScribbleSup [18], Superpixels algorithm and scribble annotations are combined in this study to generate pseudo masks as segmentation proposals, thus making the network converge fast and achieving a good performance. Fig. 2 [a,c] shows the scribble annotations and results of Superpixels, where the number of superpixels per image is 50 in Fig. 2 [a] and 80 in Fig. 2 [c]. The corresponding pseudo masks are shown in Fig. 2 [b,d]. It can be seen clearly from the figure that the pseudo mask provides more annotated pixels than scribble annotations. However, there are some incorrectly marked pixels in the pseudo mask, as a result of which the incorrectly labeled pixels may affect the segmentation performance. To address this issue, we develop a centroid loss inspired by the classic K-means algorithm. This will be discussed in the methodology section.

In this paper, an application is developed where scribbles and pseudo masks are applied to train a convolutional network for the semantic segmentation of images involved in our two tasks. In our application, the scribbles and pseudo masks are applied to train the network to propagate the category information from the labeled pixels to unlabeled pixels. It achieves a satisfactory performance on both tasks, and our main contributions are summarized as follows:

- A centroid loss is developed by integrating the clustering approach into semantic segmentation, and we assess its performance on our two tasks;
- We develop a Mean Square Error (MSE) term loss function, cooperating with partial cross-entropy loss, to refine the segmentation results;
- We make use of the centroid loss in the Attention U-Net [23], and the model achieves good performance in our two tasks.

2 Related Works

2.1 Defect Detection Approaches

Recently, there has been some literature that focuses on applying the deep learning technique to conduct corrosion inspection [24, 25, 26, 28]. Petricca et al. [28] proposed a Deep Learning approach for automatic metal corrosion (rust) detection. In this work, the authors focused on corrosion image classification. An image showing the corroded area was considered as rust, while without corroded area was non-rust. Ortiz et al. [25] proposed a system which can be used to detect corrosion or coating breakdown from vessel

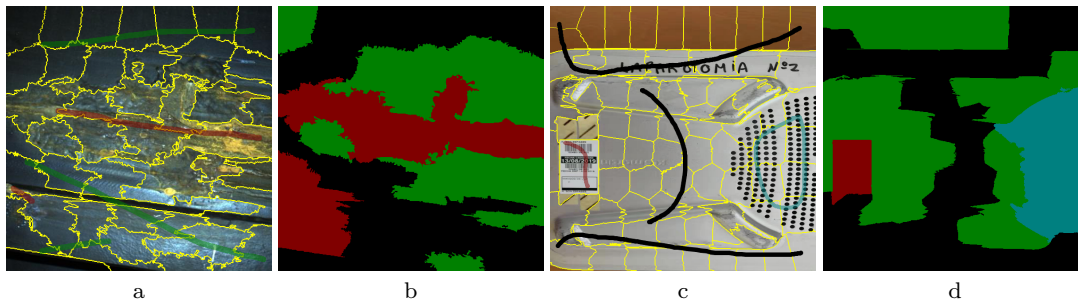


Fig. 2 Weak annotation example. Image a and c show the scribble ground truth and Superpixels segmentation result, and b and d show the pseudo masks. For the scribble annotations, in the image a, the red scribbles indicate corrosion, and green scribbles indicate background; in the image c, the black scribbles denote background, the red scribble denotes tracked label, and the blue scribble denotes internal filter. For the pseudo mask, in the image b, the red pixels represent corrosion, black pixels represent background, and the green pixels represent unlabeled pixels; in the image d, the red pixels indicate the tracked label, the blue pixels indicate the internal filter, and the definition of other colors is same to b.

images. In their work, an artificial neural network was constructed to detect corrosion with the assistance of a Micro-Aerial Vehicle. The configuration of a varying number of hidden neurons was analyzed to determine the optimal configuration of the classifier, while the information collected from RGB, HSV color space, and center-surround differences texture was combined as features to train the network.

Subsequently, Ortiz et al. [26] conducted a work based on two well-known object detection techniques, namely, Faster R-CNN [8] and Single Shot MultiBox Detector (SSD) [20], to detect the corrosion occurring to vessel structures. The two approaches were fine-tuned with VGG-16 [31] network. According to the experimental results, Faster R-CNN performed better in general and produced more accurate detection results. In order to improve the accuracy of detection, in [24], the fully convolutional network for semantic segmentation (FCN) [21] was applied to detect corrosion at the pixel level for vessel structures. Since the corroded area appears to be tiny in some images, it can lead to an imbalance during training. Allowing for this, different loss functions were applied to improve the segmentation performance. More precisely, Focal Loss [19], Dice Loss [22], Sigmoid, and Softmax Cross-Entropy Loss were employed to train the segmentation network. Ultimately, Focal Loss was identified as capable to produce the best performance for their task.

2.2 Weakly Supervised Semantic Segmentation

Although the fully supervised segmentation approaches based on DCNN can achieve an excellent performance, it requires plenty of pixel-wise annotations, which is very costly in practice. Recently, researchers have paid attention to the use of weak annotations for carrying out semantic segmentation, for example, image tags [6, 16, 38], bounding boxes [15, 27], and scribbles [14, 18, 33, 34, 37].

As for the WSSS approaches involving image tags,

with only image tags made available, most methods are based on the Class Activation Maps (CAMs) [36] as obtained from a classification network. In [6], an Attention-based Dropout Layer (ADL) was developed to obtain the entire outline of the target from the CAMs. The ADL relies on the self-attention mechanism to process the feature maps. It performs two tasks. One is to hide the most discriminating parts in the feature maps for capturing the additional target contour, and the other is to highlight the information field for improving the recognition ability of the model. In another work [38], the focus was also placed on how to obtain better CAMs. This work aimed at solving the incorrect high response in the CAMs through a linear combination of multi-dimensional CAMs. While a three terms loss function was proposed in [36] to seed, expand, and constraint the object regions progressively when the network is trained. Their loss function was based on three guiding principles: to seed with weak localization cues, to expand objects based on the information about which classes can occur in an image, and to constrain the segmentation to coincide with object boundaries.

The bounding boxes are another commonly used weak supervised annotations for semantic segmentation. In [15], GraphCut and Holistically-nested edge (HED) boundary algorithms were combined to refine the bounding boxes ground truth and predict the results while the refined ground truth was used to train the network iteratively. Similarly, in [27], the authors developed a WSSS model using bounding box annotations. Firstly, a segmentation network based on DeepLab-CRF model to obtain a series of coarse segmentation results, and secondly, a dense Conditional Random Fields (CRF) was used to facilitate the predictions and preserve object edges. In their work, they also tried to apply Expectation-Maximization (EM) method for semantic segmentation under the weakly supervised setting. The experimental results showed that, by using bounding boxes annotations, the network could obtain a good segmentation performance.

It is easy to set the scribble annotations as

there are only a few marked pixels provided in the segmentation ground truth. Such a weak annotation has already been developed in interactive segmentation with the GraphCut [4], Random Walk [9], and topological constraints [2]. These approaches require the user to provide annotations iteratively. As an improvement, [34] proposed two regularized terms based on Normalized Cuts and CRF, respectively. In this work, there were no extra MRF/CRF inference steps explicitly generating masks, and their two loss terms were trained jointly with a partial cross-entropy loss function. As a result, their approach produced a comparable performance to those fully supervised approaches. Another work [14] proposed a penalty in the loss function to enforce inequality constraints, which could avoid expensive Lagrangian dual iterates and proposal generation. Their loss function was proposed to constraint on the network output using inequality, which could leverage unlabeled data and guide the training process with domain-specific knowledge. As a result, their approach could reach a level of fully supervised segmentation performance.

In the case of semantic segmentation, one important characteristic is that targets of the same category within the same image show some similarities, i.e., the shared attributes of texture and color. Although the weak annotations cannot provide enough accurate ground truth like fully supervised segmentation, the scribble annotations can be regarded as a set of seeds to learn the shared attributes. Inspired by these approaches, a centroid loss is proposed in this study to calculate a set of centroids using weak annotations (scribbles) and an MSE-term loss is developed to cooperate with the partial cross-entropy loss to produce a refined segmentation results. Apart from that, a joint training strategy is applied to minimize the whole loss function, which leads to a competitive results for our two tasks.

3 Methodology

As shown in Figure 3 [A], the fully supervised semantic segmentation approaches based on DCNN applied a pixel-wise training strategy, to achieve a satisfactory performance. Though fully supervised model is powerful, it ignores the possibility that the pixels of the same category are similar to the adjacent pixels. For the WSSS problem, due to lack of accurate and sufficient pixel-wise labels, the similarity of pixels can be taken advantage of to obtain the categories of pixels. Currently, there are some works reliant on the similarity of pixels to train the WSSS network, for example, a dense CRF was used in [27], the GraphCut approach was adopted in [39], and the Superpixels algorithm was used in [18]. Inspired by these approaches, a semantic segmentation network is proposed in this study using scribble annotations,

which applies the idea from the clustering approach. As shown in Fig 3 [B], clustering is performed to assist in training the segmentation network and providing guidance on how to obtain the categories of the unlabeled pixels in the weak annotations. The centroids in model B are also derived from the weak annotations in an end-to-end model.

In this section, the methodology of our approach will be discussed. To begin with, the weak annotations of our two datasets used in Sec. 3.1. The architecture of the network will be described in Sec. 3.2, and the partial Cross-Entropy loss (L_{pCE}) will be briefly introduced in Sec. 3.3. Then in Sec. 3.4 and 3.5, the methodology of centroid loss (L_{cen}) and the MSE-term (L_{mse}) loss will be demonstrated.

3.1 The Weak annotations of Dataset

Figure 2 [a, c] shows two examples of the scribble annotations. For the Inspection dataset, as shown in Fig. 2 [a], the red and green scribbles represent corrosion and the background, respectively. While for the Quality Control dataset as shown in Fig. 2 [c], the black scribbles represent the background, the red scribbles denote the traced label, and the blue scribbles indicate the internal filter. It can be seen clearly that the scribble annotations has only a few labeled pixels used to train the network. Unfortunately, the performance of the network in our two tasks turns out to be far from satisfactory. Following the idea of previous works, in order to improve the performance, pseudo masks (segmentation proposals) are generated using the superpixels produced by Adaptive-SLIC (SLICO) [1] and scribble annotations, as shown in Fig. 2 [b,d]. More specifically, the training pixels belonging to a superpixel intersecting with a scribble are labeled with the same class as the scribble, as shown in Fig. 2 [b,d]. In Fig. 2 [b], the black pixels represent the background, the red pixels indicate corrosion, and the green pixels denote the unlabeled pixels omitted from training. In Fig. 2 [d], the definition of black and green pixels is the same as in Fig. 2 [b]. That is to say, the red pixels represent the traced label, blue pixels refer to the internal filter.

3.2 Network Architecture

U-Net is a prominent architecture of image segmentation intended for biomedical images, and it shows a good performance for natural images. In this work, similar to the Attention U-Net (AUN) [23], the attention module is embedded in U-Net for improving the segmentation ability for small targets.

At present, the attention module has been widely used in Natural Language Processing (NLP) [7, 12, 29,

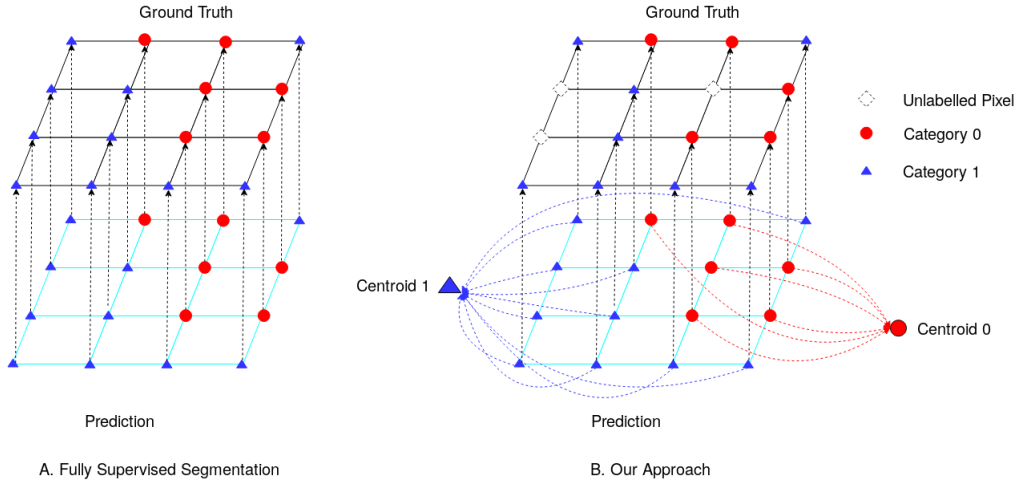


Fig. 3 The introduction of our approach. In model A, it shows the training strategy of fully supervised semantic segmentation, and model B is our approach, which integrates the idea of clustering to solve the WSSS problem.

35]. In these works, the attention module is applied to focus on the digit number that needs to be recognized in complex scenes. In the field of computer vision, an flexible trainable attention module was introduced in [11, 13, 23, 32] to improve the segmentation performance. Inspired by [23], attention gates (AGs) are integrated into the decoder parts of U-Net. To be more specific, the AGs are embedded in the U-Net to integrate the features extracted from encoder and decoder. As shown in Fig. 4, one attention gate is fed by two input tensors, with one g from the encoder and the other x from the decoder.

Figure 4 illustrates the mechanism of AGs in the network. The attention coefficient $\alpha \in [0, 1]$ identifies salient image regions and prunes feature responses to preserve only the specific task’s activation map. Unlike the Squeeze-and-Excitation (SE) Block as referred to in [11], which obtains attention weights in channels for filter selection, the AGs involved in our approach are used to calculate attention weights for spatial information. A single scalar value in α is computed for each pixel vector $x^l \in \mathbb{R}^{F_l}$, where F_l represents feature maps of layer l in the network. The AGs are expressed as follows:

$$\begin{aligned} q_{att}^l &= W_\phi^T (\sigma_1(W_x^T x^l + W_g^T g + b_g)) + b_\phi \\ \alpha^l &= \sigma_2(q_{att}^l(x^l, g; \Phi_{att})) \\ x' &= \alpha^l x^l \end{aligned} \quad (1)$$

where σ_2 represents to sigmoid activation function and σ_1 refers to the ReLU activation function. W_g , W_x , and W_ϕ indicate linear transformations, while b_g and b_ϕ denote the bias terms.

Additionally, a sub-net in the AUN is integrated to calculate the centroid loss (see Sec. 3.4). In comparison with AUN, the network shown in Fig. 5 processes two sorts of ground truth during training, scribble annotations Y_{scr} to train the sub-net for proper centroid predictions, and pseudo masks Y_{seg} for image segmentation. Apart from that, it yields two outputs, a set of centroids P_{cen} and the image segmentation

results P_{seg} . In the experimental part, the segmentation network is trained by using different weak annotations (scribbles or pseudo masks), while the sub-net is only trained by using scribble annotations. Therefore, for different experiments, the content of Y_{scr} and Y_{seg} is different. For the experiments on pseudo mask annotations, Y_{scr} represents the scribble annotations, and Y_{seg} refers to the pseudo masks. While for experiments on scribble annotations, both Y_{scr} and Y_{seg} represent scribble annotations.

The sub-net is embedded in the intermediate part of the network. As shown in Fig. 5, the sub-net consists of three blocks, each of which is comprised of a fully connected layer, a batchnorm layer, and a ReLU activated function. The shape of P_{cen} is $N \times C \times M$, where N represents the batch size, C indicates the number of categories, and M denotes the dimension of centroid features. To compute the centroids, we consider using the features of the final layer of the network and RGB color information of the input images. More specifically, for the use of CNN features, M equals to C because the dimension of the output of the last layer is C . Due to the poor performance in color clustering using RGB color features alone, the CNN features and RGB color are combined as the centroids features. In this way, M equals $C + 3$. The shape of P_{seg} is $N \times C \times H \times W$, where (W, H) is the size of the input image.

3.3 Partial Cross-Entropy Loss

Given a C -class problem and a training set Ω , comprising a subset Ω_L of labeled pixels and a subset Ω_U of unlabeled pixels, the Partial Cross-Entropy Loss L_{pCE} , widely used in weakly supervised image segmentation, computes the cross-entropy only for labeled pixels $p \in \Omega_L$, ignoring $p \in \Omega_U$:

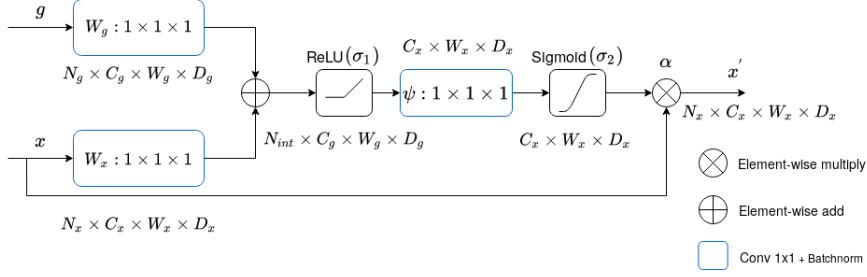


Fig. 4 The schema of attention gates (AGs). The AGs are used to calculate an attention coefficient α using the features of encoder g and decoder x . Spatial regions are selected by analyzing the semantic activation from x and the contextual information provided by g . Since the architecture of U-Net is symmetrical, so the dimension of g and x is identical, so that they can be added directly. First of all, a pixel-wise sum operation is performed to combine two input features. Secondly, a ReLU activation function, a convolutional layer with 1×1 kernel, and a batchnorm layer are applied to adapt the features. Thirdly, the spatial attention coefficients α are obtained using a sigmoid function. Finally, the input tensor x obtained from the decoder is multiplied with the α to obtain the output x' .

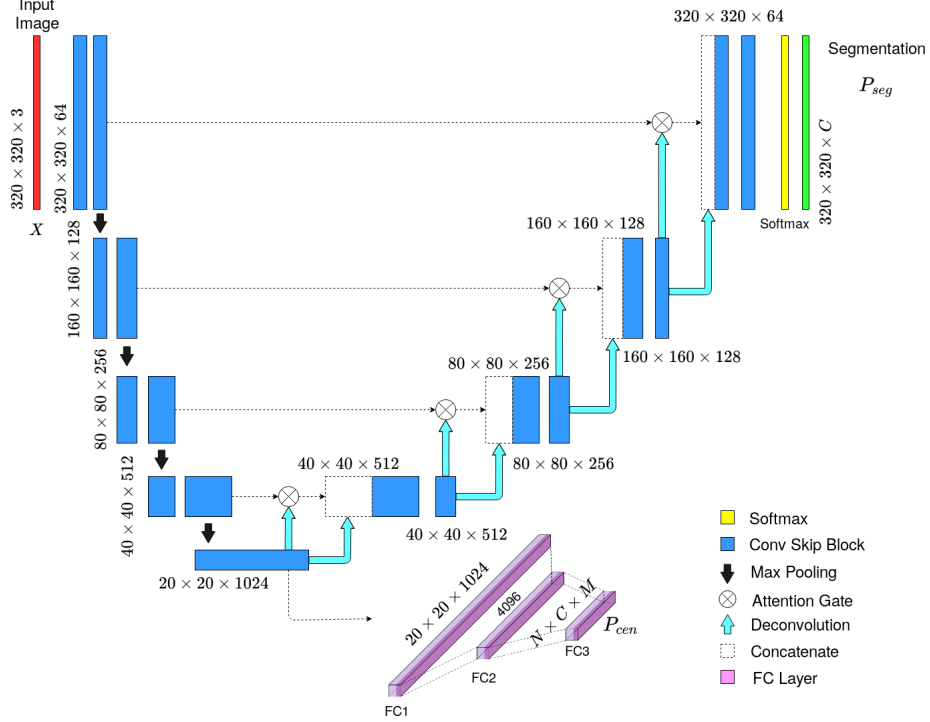


Fig. 5 Schematic description of the Centroids AUN model. The size decreases gradually by a factor of 2 at each scale in the encoding part and increases by the same factor in the decoding part. In the latter, AGs are used to help the network focus on the areas of high-response in the feature maps. The *Conv Skip* block is the *skip connection* of ResNet [10]. In this figure, N indicates the batch size, C denotes the number of classes and M represents the dimension of feature space for centroid.

3.4 Centroid Loss

$$L_{pCE} = \sum_{c=1}^C \sum_{p \in \Omega_L} -y_{g(p),c} \log y_{s(p),c} \quad (2)$$

where $y_g(p), c \in \{0, 1\}$ represents the ground truth and $y_s(p), c$ refers to the segmentation results. In our case, and for L_{pCE} , $\Omega_L^{(1)}$ is defined as the pixels labeled in pseudo-masks, while $y_s(p), c$ is as supplied by the softmax final network layer.

Although the performance of the network is decent, when trained using pseudo masks, we notice that segmentation performance depends on the quality of the pseudo masks and hence on the quality of super-pixels, i.e., how they adhere to object boundaries. The Centroid Loss function is introduced in this section for the purpose of avoiding the dependence of this kind and improving the outcome of segmentation.

In practice, this loss function actually implements a clustering process similar to K-means algorithm. Briefly speaking, K-means iteratively calculates a set of centroids μ_c for the considered number of clusters/classes, and associates the samples with the

closest clusters in feature space, thus minimizing the intra-class variance until convergence. For the scribbles supervised image segmentation, this problem can be regarded as a process of given some pixels labels, which is used to calculate centroids for every category, and clustering the pixels of entire image with these centroids. Different from other DCNN-based clustering approaches, where K-means is reformulated as a neural network optimizing the intra-class variance loss by means back-propagation-style scheme. In this work, we define the centroid loss L_{cen} as a cross-entropy loss considering in this case $\Omega_L^{(2)}$ as the set of pixels coinciding with the scribbles:

$$L_{cen} = \sum_{c=1}^C \sum_{p \in \Omega_L^{(2)}} -y_{g(p),c} \log y'_{s(p),c} \quad (a)$$

$$y'_{s(p),c} = \frac{\exp(d_{p,c})}{\sum_{c'=1}^C \exp(d_{p,c'})} \quad (b)$$

$$d_{p,c} = \frac{\|f_p - \mu_c\|_2^2}{\sum_{c'=1}^C \|f_p - \mu'_{c'}\|_2^2} \quad (c)$$

where: (1) f_p indicates the features of pixel p , and (2) μ_c denotes to the centroid predicted for class c , i.e. $\mu_c \in P_{cen}$. Equ. 3 is applied to transform the process of minimizing the distances from samples to centroids to a process of searching for the clustering with the highest probability based on the softmax formulation adopted.

3.5 Full Loss Function

Since L_{pCE} applies only to labeled pixels and L_{cen} is also restricted to a subset of image pixels, which are the pixels coinciding with scribbles. Then, we add a loss term in the form of a MSE loss L_{mse} , which calculates the normalized distance d between the segmentation results $p_{seg,c}$ with category C and its corresponding centroid $p_{cen,c}$. Therefore, over all categories, L_{mse} can involve all pixels of image. The L_{mse} is expressed as follows:

$$L_{mse} = \frac{\sum_{c=1}^C \sum_{p \in \Omega_L^{(3)}} d_{p,c}}{N \cdot C \cdot |\Omega_L^{(3)}|} \quad (4)$$

where N represents the batch size and $|A|$ stands for the cardinality of set A .

Finally, the complete loss function, to be calculated for every image in the training batch, is obtained as:

$$L = L_{pCE} + \lambda_{cen} L_{pcen} + \lambda_{mse} L_{mse} \quad (5)$$

where λ_{cen} and λ_{mse} are the trade-off constants.

4 Experiments and Discussion

In this section, several experiments are conducted on our two tasks under standard evaluation conditions where the results of using our approach can be reported. The environment of our experiments will be introduced in Sec. 4.1. In Sec. 4.2, a discussion will be conducted around the feature space of centroid loss. Besides, an analysis will be conducted in Sec. 4.3 regarding the effect of each part of our loss function on segmentation performance. Sec 4.4 is devoted to discussing the impact of weak annotations on the segmentation performance. Then, in Sec 4.5, the performance of our approach is compared against two previously-proposed approaches. Finally, the paper is conclude with some examples of our segmentation and clustering results provided in Sec. 4.6.

4.1 Experimental Environment

Datasets and Evaluations.

The test set obtained from the Quality Control dataset and Inspection dataset is applied to evaluate the performance of our approach. The Quality Control dataset contains 484 images in total, two thirds of which are designated for training and the rest are intended for testing. For the Inspection dataset comprised of 241 images, the same strategy is adopted to split the dataset.

As for the Inspection dataset, the network is evaluated for its segmentation performance with the scribble annotations and the pseudo masks as ground truth. The scribble annotations are labeled using the scribbles of 4 different widths, which are 2, 5, 10, and 20 pixels, respectively, while the boundaries of objects or ambiguous regions are avoided to mark. Meanwhile, some comparative experiments on using the pseudo masks generated by the different numbers (30, 50, and 80) superpixels per image are conducted to assess the performance of our approach. In order to identify the unlabeled pixels in the ground truth, they will change to 255 during training, which means that these pixels are ignored from the calculation of the loss value and thus do not participate in back-propagation.

Unfortunately, the network training by scribble annotations produces a very poor performance on the Quality Control dataset, despite the ultimate convergence. Thus, only pseudo mask annotations are applied to train the segmentation network and scribble annotations (20 pixels width) are used to train the centroids sub-net in the Quality Control task.

In Fig. 6, some examples of weak annotations with different settings from our two datasets are shown.

Evaluation Metric.

As a convention, the fully supervised ground truth is

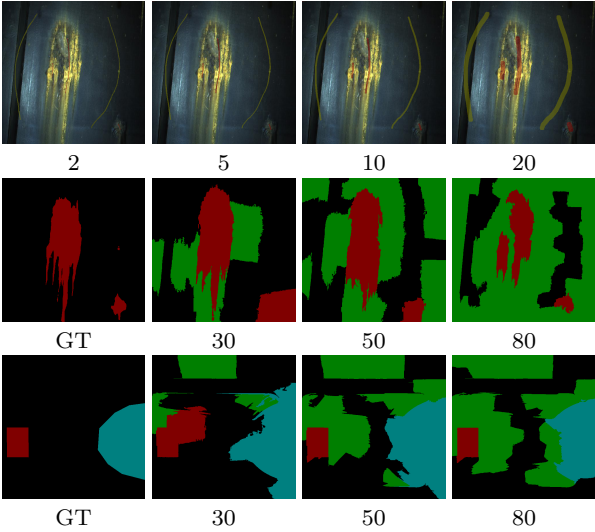


Fig. 6 The examples of weak annotations. In this figure, the first row displays the examples of scribble annotations with a varying width in the inspection dataset, where the width of scribble annotations is 2, 5, 10, and 20 from left to right, respectively. In the second and third row, the left image shows the fully supervised ground truth. Then, the remaining images are the examples of pseudo masks generated by a varying number of superpixels (30, 50, and 80). The definition of color in the pseudo masks is no different than in Fig. 2.

used to evaluate the performance of our approach, and the mean Intersection Over Union (mIOU) is calculated as a metric for comparison. Formally, let n_{ij} be the number of pixels of class i fall into class j , where there are n_c different classes, let $t_i = \sum_j n_{ij}$ be the total number of pixels of class i . The mIOU can be obtained as follows:

$$mIOU = \frac{1}{n_{cl} t_i + \sum_j n_{ji} - n_{ii}} \sum_i n_{ii} \quad (6)$$

in order to precisely represent the quality of weak annotations, we compute a weak mIOU (wmIOU) based on Equ. 6 using the weak (scribble and pseudo mask) annotations and fully supervised ground truth.

Besides, the mean Recall and mean Precision are calculated to evaluate the performance in segmentation and clustering. In our experiments, the True Positive (TP) and False Positive (FP) samples are obtained from the segmentation or clustering results, which refers to the predicted pixels that are correct or incorrect according to the fully supervised ground truth. In this way, the mean Recall (mRec) and mean Precision (mPrec) are expressed as follows:

$$mRec = \frac{\sum_{m=1}^M \frac{TP}{TP+FN}}{M} = \frac{\sum_{m=1}^M \frac{TP}{T_m}}{M} \quad (7)$$

$$mPrec = \frac{\sum_{m=1}^M \frac{TP}{TP+FP}}{M} = \frac{\sum_{m=1}^M \frac{TP}{P_m}}{M}$$

where TP , P_m , T_m , and M represent the number of true positive samples, predicted positive samples, positive samples in the ground truth, and images, respectively.

Details of implementation.

All experiments are conducted on the Pytorch platform which operates in a PC fitted with an NVIDIA GeForce RTX 2080 Ti graphic card, a 2.9GHz 12-core CPU with 32 GB RAM, and Ubuntu 64-bit. Our network is initialized by means of normalized distribution, and the weights of our network are updated at a 10^{-4} learning rate for 200 epochs. During training, we randomly crop the input image as data augmentation. A joint training strategy is used to train the AUN for semantic segmentation and the sub-net for clustering in an end-to-end module. The best possible results are obtained, with the balance parameter λ_0 and λ_1 are set to 1. The batch size is 8 for all experiments, and the size of the input image is 320×320 , which is the best configuration for our GPU.

The Setting of Comparative Experiments.

As mentioned before, the variables used in the experiments include the width of scribble annotations, the number of superpixels per image used to generate pseudo mask, and the feature space of centroids. In Tab. 1, the variations of our experiments are summarized and the names are defined to ease the further expression. For the baseline of our experiments, only L_{pCE} is used and the fully supervised approaches are adopted, as shown in Tab. 2.

In order to analyze the effect of each part of our loss function, three groups of experiments are conducted, where Group 1 (G1) indicates the network only training by L_{pCE} , Group 2 (G2) denotes the network training by L_{pCE} and L_{cen} , and Group 3 (G3) represents the network training by the full loss function defined in Equ. 5.

Additionally, there are number of previous approaches aimed at solving the WSSS problem through a modified loss function, for instance, Constrained-CNN Loss (L_{size}) [14] and Seed, Expand, and Constraint (SEC) Loss (L_{sec}) [16]. Different from their original works, their loss function were adopted to train the AUN for comparison with our approach. The loss function of the two approaches are shown in Equ. 8. For L_{Size} , the *Individual Size* loss was applied, which obtains the best performance in the original work. The uncertainty factor in L_{Size} is set to 0.1, while λ_{size} for L_{Size} Loss is $1e-3$. L_{sec} consists of three terms, which are the Seed loss (L_{seed}), the Expand loss (L_{expand}), and the constraint loss ($L_{constraint}$). In our case, the scribble annotations are applied for L_{seed} . For L_{expand} and $L_{constraint}$, we adopt the same configuration to the original work. In the end, we we

report mIOU over the test set of our two tasks as the performance comparison.

$$\begin{cases} L_{size} &= L_{pCE} + \lambda_{size}L_{Size} \\ L_{sec} &= L_{seed} + L_{expand} + L_{constraint} \end{cases} \quad (8)$$

4.2 Discussion of Feature Space

Generally speaking, color features are widely used in image semantic segmentation. In [30], a standard Gaussian kernel over RGBXY feature space was used to calculate a Laplacian matrix. While in [17], the same feature space was used to obtain a pair-wise energy function as an optimized target. Different from color information, the features extracted from the top layers of CNN carry semantic information. Due to downsampling operations such as pooling, these features lost such detailed information as texture, color, shape, and spatial relationship. To address this problem, RGB color features are integrated with CNN features to compute L_{cen} and L_{mse} .

As mentioned in Sec. 3.2, the shape of P_{cen} is $N \times C \times M$. As only the features extracted from the last layer of network are utilized, M equals the number of category C , where C is 2 (Corrosion and Non-Corrosion) in the Inspection task, and C is 7 in the Quality Control task. After the integration with RGB color space, M equals to $C + 3$. As usual, the value of RGB color space is either much higher or lower than that of CNN features. Therefore, the RGB values are normalized to ensure that its value ranges between 0 to 1. Then, CNN features are integrated with normalized RGB features to calculate L_{cen} and L_{mse} .

As shown in Tab. 4, the performance of our approach is evaluated using scribble annotations as segmentation ground truth on the Inspection dataset. It can be seen clearly from the table that the segmentation and clustering mIOU of experiments E-SCR*-NRGB is lower than the mIOU in experiments E-SCR*-N, and there is a big gap in performance, which suggests that the RGB features fail to improve the performance of our approach in segmentation and clustering by using scribble annotations supervision on the inspection dataset.

Besides, Tab. 5 lists the experimental results in terms of mIOU with pseudo masks as segmentation ground truth. For both datasets, unlike the results shown in Tab. 4, the performance of experiments E-SCR20-SUP*-NRGB is similar to that of experiments E-SCR20-SUP*-N. Additionally, the mIOU of some experiments where the integrated features are used is even higher than if only CNN features are used. By observing the experimental performance achieved by using different annotations, it can be found out that our approach with the integrated features

requires more marked pixels to achieve a good segmentation and clustering performance. In contrast, the use of CNN features only simply requires scribbles annotations to produce a good performance for the inspection task.

Furthermore, by observing the corrosion area in the inspection dataset, it can be found out that different corrosion areas are different in appearances on the same image and there is a similar appearance in the background. In this way, the corrosion category shows heterogeneity between each other and shows homogeneity to the background. Therefore, the color space features cannot become effective features for classification. For a scientific demonstration, the distribution of pixels of the scribble annotations in the RGB color space is shown in the first row of Fig. 7 [right]. As can be seen from the figure, a large proportion of pixels in corrosion and non-corrosion area overlap, which makes it difficult to find two centroids for the correct classification of the corrosion and non-corrosion pixels. In the first row of Fig. 7 [left], it is clearly seen that the color of the corrosion and non-corrosion are is highly similar.

Meanwhile, in the Quality Control dataset, although the color of the targets in the same category is generally consistent, it is similar to the color of the background. For example, as shown in the second row of Fig 7 [left], the color of part of the Internal Filter is the same as the box, and it can be seen that the points of the Internal Filter and the points of background coincide in the right image of the second row of Fig 7. Identical to the Inspection dataset, the RGB color space is not suitable for the Quality Control task. Thus, RGB color space makes it difficult to carry out our two tasks.

Finally, as shown in Tab. 4 and Tab. 5, our approach using CNNs features obtains higher mIOU than using the integrated features in most of the experiments. Thus, CNN features are adopted to perform future experiments.

4.3 The Effect of Centroid Loss

To analyze the effect of L_{cen} and L_{mse} on the segmentation results, the performance of each group experiment is compared.

In Table 4, the mIOU of experiments in G2 is significantly higher than that of experiments in G1, where the gap of the maximum mIOU in G1 and G2 is 0.2066. While with L_{mse} used, the segmentation performance of the G3 experiments is superior to that of G2 experiments under the condition that the same width is used to scribble annotations.

Furthermore, in Tab. 5, the segmentation performance is improved by adding L_{cen} in G2 compared with experiments in G1, and the performance of G3 experiments is superior to that of G2 experiments for

Table 1 The variations of the comparative experiments.

Name	Scribbles width	Number of Superpixels	Features space of centroids
E-SCR2-N	2	-	CNN
E-SCR2-NRGB	2	-	CNN & RGB
E-SCR5-N	5	-	CNN
E-SCR5-NRGB	5	-	CNN & RGB
E-SCR10-N	10	-	CNN
E-SCR10-NRGB	10	-	CNN & RGB
E-SCR20-N	20	-	CNN
E-SCR20-NRGB	20	-	CNN & RGB
E-SCR20-SUP30-N	20	30	CNN
E-SCR20-SUP30-NRGB	20	30	CNN & RGB
E-SCR20-SUP50-N	20	50	CNN
E-SCR20-SUP50-NRGB	20	50	CNN & RGB
E-SCR20-SUP80-N	20	80	CNN
E-SCR20-SUP80-NRGB	20	80	CNN & RGB

Table 2 The baseline of experiments.

Name	Loss Function	Scribbles width	Number of Superpixels	Supervision
E-SCR2	L_{pCE}	2	-	Scribbles
E-SCR5		5	-	Scribbles
E-SCR10		10	-	Scribbles
E-SCR20		20	-	Scribbles
E-SUP30		-	30	Pseudo masks
E-SUP50		-	50	Pseudo masks
E-SUP80	-	80	Pseudo masks	
E-FULL	L_{CE}	-	-	Full

both our two tasks. Therefore, by adding L_{cen} and L_{mse} , the segmentation mIOU is gradually improved for our two tasks.

Regarding the clustering performance, the mIOU of experiments in G3 is also higher than that of experiments in G2. In addition, it can be found out in Tab. 4 and Tab. 5 that the clustering mIOU in some G2 experiments (E-SCR20-SUP30-N on both two datasets and E-SCR20-SUP80-N on Quality Control dataset) is higher than in G3 experiments, while the segmentation mIOU in G2 is lower than in G3. It is suggested that L_{mse} , in some experiments, causes the clustering performance to deteriorate but enhances the segmentation performance.

Overall, through the addition of L_{cen} and L_{mse} , the segmentation performance is improved progressively on our two tasks, and the segmentation performance is superior to the clustering performance.

4.4 The Impact of Weak Annotations

In this section, the performance of our approach is assessed under different weak annotations and a discussion is conducted about the impact of weak annotations on the performance of our approach. Since the definition of the quality of weak annotations is subjective and ambiguous, the wmIOU is calculated using weak annotations and fully supervised ground truth for the purpose of evaluation. To analyze the

effect that weak annotations have, the curves of mIOU, recall, and precision value are plotted under different weak annotations supervision for our two tasks, as shown in Fig. 8. According to these figures, the curves of mIOU, recall, and precision of G3 experiments are higher than others in general.

As for the Inspection task, in Fig.8 [a], it can be seen that the segmentation mIOU curves of our approach maintain a relative level of stability, while the curve of baseline (G1) shows a similar shape to the curve of wmIOU. For the Quality Control task, the segmentation performance exhibits a positive relation with the wmIOU value shown in Fig. 8 [d]. By comparing our two tasks, it can be known that the Inspection dataset is binary dataset, which means it is sufficient to detect corrosion. In contrast, the Quality Control dataset is a multi-category task, and it is more complex than the Inspection dataset. Therefore, the information contained in scribble annotations is insufficient for our approach to produce a good performance in segmentation. However, our approach can obtain a higher mIOU than the baseline shown in Fig. 8 [d]. Thus, the centroid loss can help to improve the segmentation performance, despite the fact that its performance is also affected by the quality of weak annotations.

Additionally, by observing the precision curves corresponding to Fig. 8 [c,f], the precision curves of weak annotations show a sharp decline when the weak annotations shift from scribbles to pseudo masks. As seen in the pseudo masks in the second and third

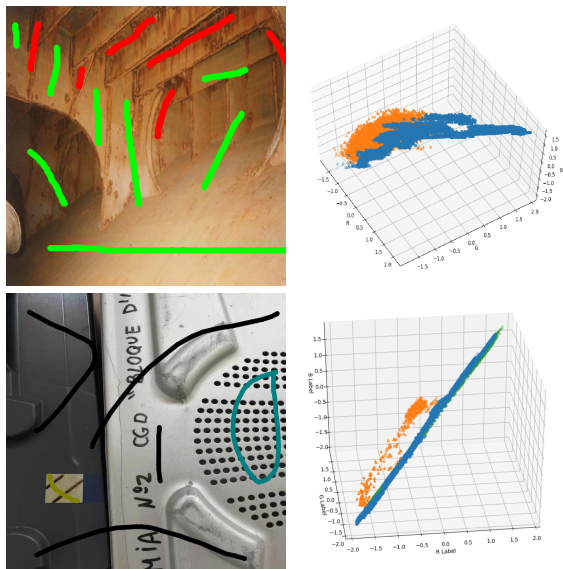


Fig. 7 Discussion of Centroid Feature Space. The left column shows the scribbles ground truth, and the right column shows the distribution of pixels marked by the scribble annotations in RGB color space. The above row is an example obtained from the Inspection dataset, and the below row is an example collected from the Quality Control dataset. In the top right figure, the blue points indicate the pixels of background scribbles, and the orange points denote the pixels of corrosion scribbles. In the bottom right figure, the blue points indicate the pixels of background scribbles, the orange points denote the pixels of paper tape, and the green pixels refers to the pixels of Internal Filter.

row of Fig. 6, when the number of superpixels is 30, the pseudo masks contain lots of incorrectly marked pixels, and the number of marked pixels is significantly higher than that of the scribble annotations. Thus, the precision curves of weak annotations show a downward trend shown in Fig. 8 [c,f] while the recall curves exhibit an upward trend Fig. 8 [b,e]. In this situation, we can see that the curves of three metrics of G3 experiments are higher than that of G2 experiments, and the curves of G3 and G2 experiments are higher than that of G1 in general. Thus, it can be judged that our method is more effective in achieving a good performance when incorrectly marked pixels are contained in pseudo masks than the baseline.

In summary, for our two tasks, the quality of weak annotations still directly affects the segmentation performance. However, the full centroid loss can obtain a better segmentation than only using partial cross-entropy. On the other hand, the mislabeled pixels have less impact on the segmentation performance of our approach.

4.5 Comparative Results

In Table 3, the performance of our approach is compared with that of two previous approaches on the test set of our two tasks, including L_{size} [14] and L_{sec} [16], and the weak annotations in this table have

the same definition as in Tab. 2. It can be seen clearly that our approach outperformed almost all previous approaches.

As for the Inspection task, the network trained by L_{size} produces a similar performance to our approach when the scribble annotations are used. However, our approach obtains a higher mIOU in SCR2, SCR5, and SCR10 experiments. The performance of L_{sec} is clearly inferior to others with scribbles annotations used. When the pseudo masks are applied, the performance of the three approaches shows no significant difference. However, our approach obtains the highest mIOU (0.7542). As for the Quality Control task, the mIOU of our approach is higher than that of the other two approaches.

Thus, it can be concluded that our approach can perform better on our two tasks compared with L_{size} and L_{sec} .

4.6 Experimental Results

As discussed in Sections 4.3 and 4.4, the network training by the whole centroid loss (G3) can produce the best segmentation performance. The segmentation and clustering performance metrics of G3 experiments are shown in Tab. 6, including mean recall, mean precision, and mIOU. In order to improve the segmentation performance, dense CRF is taken as the post-processor on the segmentation results.

For the Inspection task, the experiment E-SCR20-SUP50-N leads to the best segmentation mIOU (0.7542), as shown in Tab. 6. After dense CRF, the mIOU reaches 0.7859, while the performance gap with the E-FULL is 0.0474. Although the experiment E-SCR20-SUP30-N obtains the highest recall value (0.7937), however, its precision is very low (0.6981), and mIOU is merely 0.6919. In other words, the segmentation result of E-SCR20-SUP30-N contains more incorrect predictions than E-SCR20-SUP50-N.

As for the Quality Control task, the segmentation mIOU of E-SCR20-SUP80-N is the highest among all experiments. By comparing the values of recall, it can be found out that the experiment E-SCR20-SUP30-N obtains the best recall, while its precision is the lowest. As for E-SCR20-SUP80-N, the value of precision is 0.8428, which is slightly lower than the maximum of 0.8439. After dense CRF, the final segmentation mIOU is 0.7707.

The experimental results shown in Table 6 evidence that the experiments of E-SCR20-SUP50-N and E-SCR20-SUP80-N can produce the best segmentation performance on Inspection and Quality Control dataset, respectively. Compared with the baseline (G1), the presence of fully centroid loss is conducive to training and improving accuracy significantly. Figure 7 shows the segmentation and clustering results of some examples in the test set of

Table 3 Performance comparison on our two tasks using different approaches. Best performance are in bold.

Dataset	Weak Annotation	Size Loss [14]	SEC [16]	Ours
Inspection	SCR2	0.6098	0.4366	0.6995
	SCR5	0.6537	0.4372	0.7134
	SCR10	0.6754	0.5486	0.7047
	SCR20	0.6909	0.5624	0.6904
	SUP30	0.7068	0.6397	0.6919
	SUP50	0.6769	0.7428	0.7542
Quality Control	SUP80	0.7107	0.6546	0.7294
	SUP30	0.4724	0.5808	0.7030
	SUP50	0.4985	0.6262	0.7291
	SUP80	0.5051	0.6918	0.7679

the Inspection task. It is clear seen that the results obtained from using our approach are similar to the results of E-FULL. In addition, the clustering results are presented in Fig. 7, and it contains more incorrect predictions than segmentation results. As for the Quality Control task, the same conclusion can be drawn from Fig. 9.

In the using of centroid loss makes it possible to train the segmentation network using a small number of marked pixels. Although the performance of our approaches is inferior to that of a fully supervised approach, it is believed that this is a reasonable gap in our two tasks, given the challenges arising from the exercise of weak annotations.

5 Conclusion and Future Work

In this paper, a weakly supervised segmentation approach based on AUN is proposed and its performance is evaluated using two real datasets collected from the vessels’ structural parts and the surgery boxes. The loss function is comprised of three terms and is jointly optimized using an end-to-end model. As has been reported in the experimental results section, our approach can achieve a satisfactory performance with a low cost of labeling work required for semantic segmentation ground truth. Under the weak annotations of varying quality, our approach can produce a good segmentation performance and reduce the negative impact of incorrect label on the segmentation results.

Though the performance gap between our approach and the fully supervised approach is insignificant, the values of recall and precision are still incomparable to the fully supervised method. With scribble annotations used for a multi-category task, such as the Quality Control task, the performance of our approach fails to meet the real-world requirements. In the future, it is necessary to close the performance gap and to improve the performance under scribble annotations supervision. In the end, it is worth trailing our approach on other segmentation architectures (such as FCN, DeepLab) and a deep backbone for

performing complicated tasks.

References

1. Achanta, R., Shaji, A., Smith, K., Lucchi, A., Fua, P., Süsstrunk, S.: Slic superpixels compared to state-of-the-art superpixel methods. *IEEE transactions on pattern analysis and machine intelligence* **34**(11), 2274–2282 (2012)
2. Bai, X., Sapiro, G.: Geodesic matting: A framework for fast interactive image and video segmentation and matting. *International journal of computer vision* **82**(2), 113–132 (2009)
3. Bell, S., Upchurch, P., Snavely, N., Bala, K.: Opensurfaces: A richly annotated catalog of surface appearance. *ACM Transactions on graphics (TOG)* **32**(4), 1–17 (2013)
4. Boykov, Y.Y., Jolly, M.P.: Interactive graph cuts for optimal boundary & region segmentation of objects in nd images. In: *Proceedings eighth IEEE international conference on computer vision. ICCV 2001*, vol. 1, pp. 105–112. IEEE (2001)
5. Chen, L.C., Papandreou, G., Schroff, F., Adam, H.: Rethinking atrous convolution for semantic image segmentation. *arXiv preprint arXiv:1706.05587* (2017)
6. Choe, J., Shim, H.: Attention-based dropout layer for weakly supervised object localization. In: *Proceedings of the IEEE Conference on Computer Vision and Pattern Recognition*, pp. 2219–2228 (2019)
7. Clark, K., Khandelwal, U., Levy, O., Manning, C.D.: What does bert look at? an analysis of bert’s attention. *arXiv preprint arXiv:1906.04341* (2019)
8. Girshick, R.: Fast r-cnn. In: *The IEEE International Conference on Computer Vision (ICCV)* (2015)
9. Grady, L.: Random walks for image segmentation. *IEEE transactions on pattern analysis and machine intelligence* **28**(11), 1768–1783 (2006)
10. He, K., Zhang, X., Ren, S., Sun, J.: Deep residual learning for image recognition. In: *Proceedings*

Table 4 Segmentation Performance of comparative experiments results of varying widths of scribble annotations. *R indicates to compute L_{cen} and L_{mse} using RGB features, while *C indicates to use the CNN features.

Dataset	Experiments	wmIOU	L_{pCE}	L_{cen}	L_{mse}	mIOU (Seg,*C)	mIOU (Seg,*R,*C)	mIOU (Clu,*R,*C)
Inspection	E-SCR2	0.2721	✓			0.3733	-	-
	E-SCR5	0.2902	✓			0.4621	-	-
	E-SCR10	0.3074	✓			0.4711	-	-
	E-SCR20	0.3233	✓			0.5286	-	-
	E-SCR2-N/NRGG	0.2721	✓	✓		0.6851	0.4729	0.3889
	E-SCR5-N/NRGG	0.2902	✓	✓		0.6798	0.4989	0.6020
	E-SCR10-N/NRGG	0.3074	✓	✓		0.6992	0.5130	0.6267
	E-SCR20-N/NRGG	0.3233	✓	✓		0.6852	0.5562	0.6164
E-SCR2-N/NRGG	0.2721	✓	✓	✓	0.6995	0.4724	0.3274	
E-SCR5-N/NRGG	0.2902	✓	✓	✓	0.7134	0.4772	0.2982	
E-SCR10-N/NRGG	0.3074	✓	✓	✓	0.7047	0.4796	0.3130	
E-SCR20-N/NRGG	0.3233	✓	✓	✓	0.6904	0.5075	0.6187	

Table 5 Segmentation Performance of comparative experiments results of varying number of superpixels of pseudo mask. *R indicates to compute L_{cen} and L_{mse} using RGB features, and *C indicates to use the CNN features.

Dataset	Experiments	wmIOU	L_{pCE}	L_{cen}	L_{mse}	mIOU (Seg,*C)	mIOU (Seg,*R,*C)	mIOU (Clu,*R,*C)
Inspection	E-SUP30	0.6272	✓			0.6613	-	-
	E-SUP50	0.6431	✓			0.7133	-	-
	E-SUP80	0.6311	✓			0.7017	-	-
	E-SCR20-SUP30-N/NRGG	0.6272	✓	✓		0.6848	0.6847	0.6859
	E-SCR20-SUP50-N/NRGG	0.6431	✓	✓		0.7447	0.7368	0.7136
	E-SCR20-SUP80-N/NRGG	0.6311	✓	✓		0.7242	0.7355	0.7127
	E-SCR20-SUP30-N/NRGG	0.6272	✓	✓	✓	0.6919	0.7071	0.7076
	E-SCR20-SUP50-N/NRGG	0.6431	✓	✓	✓	0.7542	0.7133	0.7294
E-SCR20-SUP80-N/NRGG	0.6311	✓	✓	✓	0.7294	0.7246	0.7118	
Quality Control	E-SUP30	0.4710	✓			0.5419	-	-
	E-SUP50	0.5133	✓			0.6483	-	-
	E-SUP80	0.5888	✓			0.7015	-	-
	E-SCR20-SUP30-N/NRGG	0.4710	✓	✓		0.6882	0.6889	0.6062
	E-SCR20-SUP50-N/NRGG	0.5133	✓	✓		0.7236	0.7203	0.6480
	E-SCR20-SUP80-N/NRGG	0.5888	✓	✓		0.7594	0.7337	0.6451
	E-SCR20-SUP30-N/NRGG	0.4710	✓	✓	✓	0.7030	0.6237	0.6077
	E-SCR20-SUP50-N/NRGG	0.5133	✓	✓	✓	0.7291	0.7046	0.6372
E-SCR20-SUP80-N/NRGG	0.5888	✓	✓	✓	0.7679	0.7409	0.6780	

Table 6 The results of segmentation and clustering using the full loss function (G3) on the testset. The bold numbers indicate the highest numbers of other experiments, and *CRF refers to the performance after dense CRF post-processing.

Dataset	Experiments	wmIOU	mIOU (seg)	mRec (seg)	mPrec (seg)	mIOU (clu)	mRec (clu)	mPrec (clu)	*CRF (seg)
	E-SCR2-N	0.2721	0.6995	0.6447	0.6452	0.6828	0.7663	0.5803	0.7068
	E-SCR5-N	0.2902	0.7134	0.6539	0.6542	0.7001	0.7447	0.6015	0.7212
	E-SCR10-N	0.3074	0.7047	0.6797	0.6332	0.6817	0.7741	0.5772	0.7241
	E-SCR20-N	0.3233	0.6904	0.6917	0.6081	0.6894	0.7816	0.5507	0.7172
Inspection	E-SCR20-SUP30-N	0.6272	0.6919	0.7937	0.7081	0.6987	0.7806	0.5946	0.7489
	E-SCR20-SUP50-N	0.6431	0.7542	0.7543	0.7567	0.7491	0.7725	0.6830	0.7859
	E-SCR20-SUP80-N	0.6311	0.7294	0.7452	0.7397	0.7268	0.7758	0.6200	0.7693
	E-FULL	1.0	0.8333	0.8537	0.9119	-	-	-	0.8218
Quality Control	E-SCR20-SUP30-N	0.4710	0.7030	0.7937	0.7924	0.5910	0.7600	0.6798	0.7142
	E-SCR20-SUP50-N	0.5133	0.7291	0.8298	0.8439	0.6605	0.7777	0.7332	0.7143
	E-SCR20-SUP80-N	0.5888	0.7679	0.8303	0.8398	0.6687	0.8630	0.7606	0.7707
	E-FULL	1.0	0.8604	0.8058	0.8432	-	-	-	0.8459

- of the IEEE conference on computer vision and pattern recognition, pp. 770–778 (2016)
- Hu, J., Shen, L., Sun, G.: Squeeze-and-excitation networks. In: Proceedings of the IEEE conference on computer vision and pattern recognition, pp. 7132–7141 (2018)
 - Jain, S., Wallace, B.C.: Attention is not explanation. arXiv preprint arXiv:1902.10186 (2019)
 - Jetley, S., Lord, N.A., Lee, N., Torr, P.H.: Learn to pay attention. arXiv preprint arXiv:1804.02391 (2018)
 - Kervadec, H., Dolz, J., Tang, M., Granger, E., Boykov, Y., Ayed, I.B.: Constrained-cnn losses for weakly supervised segmentation. Medical image analysis **54**, 88–99 (2019)
 - Khoreva, A., Benenson, R., Hosang, J., Hein, M., Schiele, B.: Simple does it: Weakly supervised instance and semantic segmentation. In: Proceedings of the IEEE conference on computer vision and pattern recognition, pp. 876–885 (2017)
 - Kolesnikov, A., Lampert, C.H.: Seed, expand and constrain: Three principles for weakly-supervised image segmentation. In: European conference on computer vision, pp. 695–711. Springer (2016)
 - Krähenbühl, P., Koltun, V.: Efficient inference in fully connected crfs with gaussian edge potentials. In: Advances in neural information processing systems, pp. 109–117 (2011)
 - Lin, D., Dai, J., Jia, J., He, K., Sun, J.: Scribble-sup: Scribble-supervised convolutional networks for semantic segmentation. In: Proceedings of the IEEE Conference on Computer Vision and Pattern Recognition, pp. 3159–3167 (2016)
 - Lin, T.Y., Goyal, P., Girshick, R., He, K., Dollár, P.: Focal loss for dense object detection. In: Proceedings of the IEEE international conference on computer vision, pp. 2980–2988 (2017)
 - Liu, W., Anguelov, D., Erhan, D., Szegedy, C., Reed, S., Fu, C.Y., Berg, A.C.: Ssd: Single shot multibox detector. In: European conference on computer vision, pp. 21–37. Springer (2016)
 - Long, J., Shelhamer, E., Darrell, T.: Fully convolutional networks for semantic segmentation. In: Proceedings of the IEEE conference on computer vision and pattern recognition, pp. 3431–3440 (2015)
 - Milletari, F., Navab, N., Ahmadi, S.A.: V-net: Fully convolutional neural networks for volumetric medical image segmentation. In: 2016 fourth international conference on 3D vision (3DV), pp. 565–571. IEEE (2016)
 - Oktay, O., Schlemper, J., Folgoc, L.L., Lee, M., Heinrich, M., Misawa, K., Mori, K., McDonagh, S., Hammerla, N.Y., Kainz, B., et al.: Attention u-net: Learning where to look for the pancreas. arXiv preprint arXiv:1804.03999 (2018)
 - Ortiz, A., Bonnin-Pascual, F., Garcia-Fidalgo, E.: Visual inspection of vessels cargo holds: Use

- of a micro-aerial vehicle as a smart assistant. In: IMEKO TC-19 International Workshop on Metrology for the Sea (MetroSea) (2019)
25. Ortiz, A., Bonnin-Pascual, F., Garcia-Fidalgo, E., et al.: Visual inspection of vessels by means of a micro-aerial vehicle: an artificial neural network approach for corrosion detection. In: Robot 2015: Second Iberian Robotics Conference, pp. 223–234. Springer (2016)
 26. Ortiz, A., Yao, K., Bonnin-Pascual, F., Garcia-Fidalgo, E., et al.: New steps towards the integration of robotic and autonomous systems in the inspection of vessel holds. In: Spanish National Robotics Conference (2018)
 27. Papandreou, G., Chen, L.C., Murphy, K.P., Yuille, A.L.: Weakly-and semi-supervised learning of a deep convolutional network for semantic image segmentation. In: Proceedings of the IEEE international conference on computer vision, pp. 1742–1750 (2015)
 28. Petricca, L., Moss, T., Figueroa, G., Broen, S.: Corrosion detection using ai: a comparison of standard computer vision techniques and deep learning model. In: Proceedings of the Sixth International Conference on Computer Science, Engineering and Information Technology, vol. 91, p. 99 (2016)
 29. Serrano, S., Smith, N.A.: Is attention interpretable? arXiv preprint arXiv:1906.03731 (2019)
 30. Shi, J., Malik, J.: Normalized cuts and image segmentation. *IEEE Transactions on pattern analysis and machine intelligence* **22**(8), 888–905 (2000)
 31. Simonyan, K., Zisserman, A.: Very deep convolutional networks for large-scale image recognition. arXiv preprint arXiv:1409.1556 (2014)
 32. Sinha, A., Dolz, J.: Multi-scale self-guided attention for medical image segmentation. *IEEE Journal of Biomedical and Health Informatics* (2020)
 33. Tang, M., Djelouah, A., Perazzi, F., Boykov, Y., Schroers, C.: Normalized cut loss for weakly-supervised cnn segmentation. In: Proceedings of the IEEE Conference on Computer Vision and Pattern Recognition, pp. 1818–1827 (2018)
 34. Tang, M., Perazzi, F., Djelouah, A., Ben Ayed, I., Schroers, C., Boykov, Y.: On regularized losses for weakly-supervised cnn segmentation. In: Proceedings of the European Conference on Computer Vision (ECCV), pp. 507–522 (2018)
 35. Vaswani, A., Shazeer, N., Parmar, N., Uszkoreit, J., Jones, L., Gomez, A.N., Kaiser, L., Polosukhin, I.: Attention is all you need. In: Advances in neural information processing systems, pp. 5998–6008 (2017)
 36. Wei, Y., Feng, J., Liang, X., Cheng, M.M., Zhao, Y., Yan, S.: Object region mining with adversarial erasing: A simple classification to semantic segmentation approach. In: Proceedings of the IEEE conference on computer vision and pattern recognition, pp. 1568–1576 (2017)
 37. Xu, J., Schwing, A.G., Urtasun, R.: Learning to segment under various forms of weak supervision. In: Proceedings of the IEEE conference on computer vision and pattern recognition, pp. 3781–3790 (2015)
 38. Yang, S., Kim, Y., Kim, Y., Kim, C.: Combinational class activation maps for weakly supervised object localization. In: The IEEE Winter Conference on Applications of Computer Vision, pp. 2941–2949 (2020)
 39. Zhao, X., Liang, S., Wei, Y.: Pseudo mask augmented object detection. In: Proceedings of the IEEE conference on computer vision and pattern recognition, pp. 4061–4070 (2018)

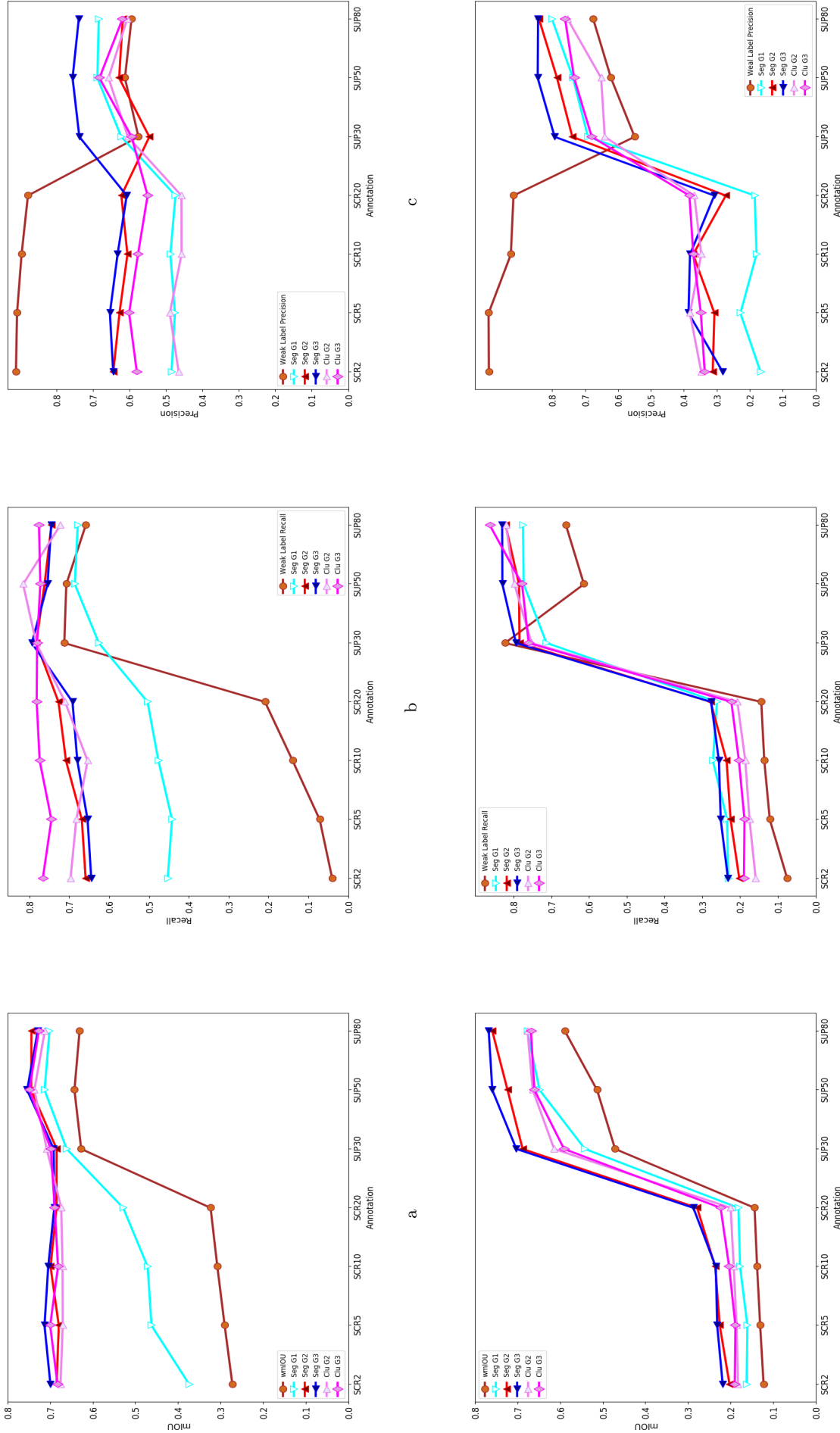


Fig. 8 The performance of our approach under different weak annotations. The first row shows the performance of our approach on the Inspection dataset. From left to right, the three figures (a,b,c) are the curves of mIOU, mean Recall, and mean Precision. The second row shows the results of Quality Control task, and the three figures (d,e,f) are arranged in the same order as the first row.

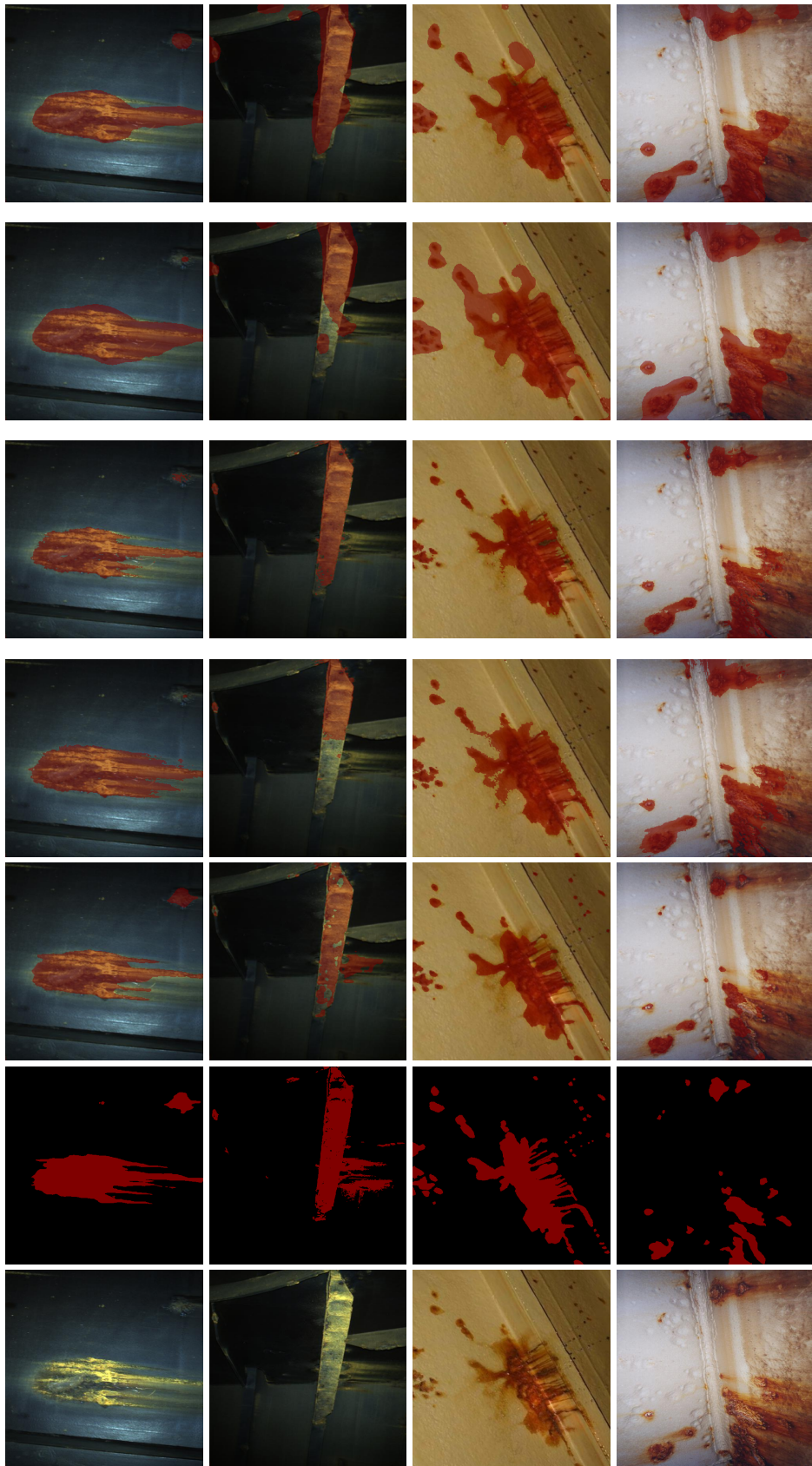


Table 7 Examples of segmentation results. The input images are shown in the first column; the second column shows the fully supervised ground truth; the third column shows the results of the fully supervised approach; the fourth and fifth columns present the examples of the segmentation results of E-SCR20-N and E-SCR20-SUP50-N after dense CRF. The last two columns show the corresponding clustering results.

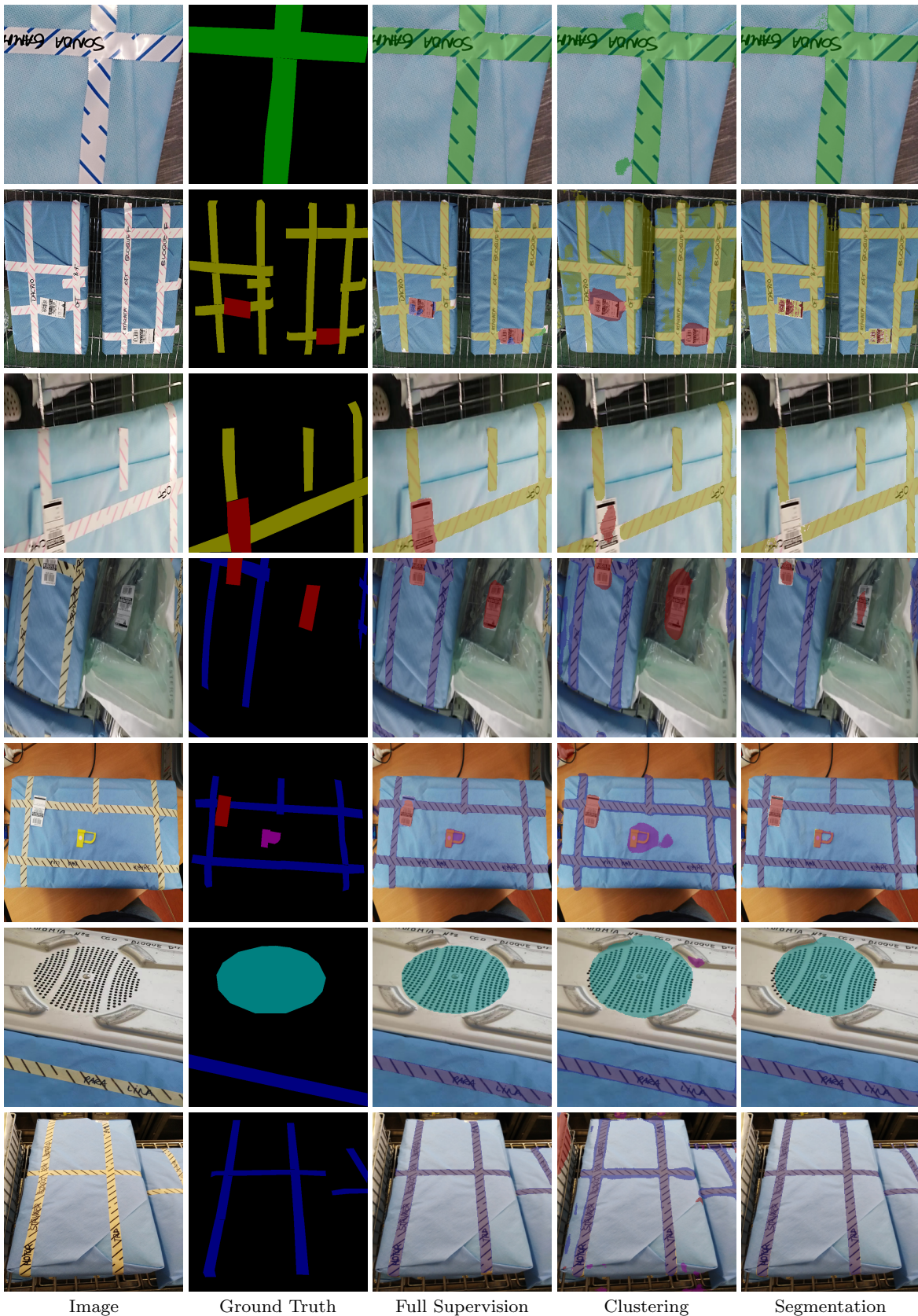


Fig. 9 Examples of segmentation results on the Quality Control dataset. The input images are shown in the first column; the second column shows the fully supervised ground truth; the third column shows the results of the fully supervised approach; the fourth column represents examples of the clustering results of E-SCR20-SUP80-N; its segmentation results obtained after dense CRF are shown in the fifth column.